Journal of Alloys and Compounds 589 (2014) 572–578

Contents lists available at ScienceDirect

Journal of Alloys and Compounds

journal homepage: www.elsevier.com/locate/jalcom

Charge and mass transport properties of $La_2Ni_{0.95}Al_{0.05}O_{4.025+\delta}$

Sang-Yun Jeon, Bhupendra Singh, Ha-Ni Im, Kyung-Pil Seong, Sun-Ju Song *

School of Materials Science and Engineering, Chonnam National University, 300 Yongbong-dong, Buk-gu, Gwang-Ju 500-757, Republic of Korea

ARTICLE INFO

Article history:
Received 5 October 2013
Received in revised form 27 November 2013
Accepted 4 December 2013
Available online 11 December 2013

Keywords:
Oxide materials
Thermal expansion
Ionic conduction
Diffusion
Electrode materials

ABSTRACT

In this work, mass and charge transport properties of acceptor doped lanthanum nickelate, $La_2Ni_{0.95}Al_{0.05}O_{4.025+\delta}$ (LNAO), were analyzed. The thermal expansion, electrical conductivity and thermoelectric power of LNAO were measured as a function of temperature in 25–1000 °C range and oxygen partial pressure (pO_2) in $-14 \leqslant \log(pO_2/\text{atm}) \leqslant -1$ range. The average thermal expansion coefficient was $13.77 \times 10^{-6}\ K^{-1}$. The electrical conductivity was analyzed in relation to the thermoelectric power to elucidate the positive deviation of the activity coefficient of hole on the basis of the delocalized electron model. The thermoelectric power measurement shows a p-type to n-type transition. The chemical diffusion coefficient ($\tilde{D}_{chem}$) and surface exchange coefficient ($k_{surf.}$) were calculated by 4-probe DC conductivity measurement and $k_{surf.}$ was slightly higher than ($\tilde{D}_{chem}$). The best-estimated hole-mobility values showed very weak temperature dependence. The results were compared with the literature results on $La_2NiO_{4+\delta}$.

1. Introduction

Mixed oxide-ion and electron conducting ceramic material $La_2NiO_{4+\delta}$ (LNO) have been reported to exhibit impressive oxide ion and p-type electronic conductivity, and high catalytic activity which make them an excellent component of some electrochemical devices [1–8]. The hyperstoichiometric LNO oxides show high oxygen diffusion coefficient and high oxygen ion conductivity, which are attributes of their crystal structure [9–12]. The structure of LNO is related to that of K_2NiF_4 and consists of alternating $LaNiO_3$ perovskite and LaO rock salt layers. The oxygen excess in LNO is associated with the incorporation of interstitial oxygen (O_i'') into the rock salt layers and holes ($h^{\cdot}$) are simultaneously created in the $LaNiO_3$ perovskite layers to maintain the charge neutrality of the system [13,14].

The oxygen nonstoichiometry significantly affects the electrochemical properties of LNO-based systems and can be varied by aliovalent doping or by substituting the host cation with smaller size cations [15–17]. The conduction mechanism in LNO-based system has been explained on the basis of both, the band conduction by delocalized electrons and polaron-hopping by localized electrons [15,18]. In our recent work, we have shown that in case of $La_2Ni_{0.95}Al_{0.05}O_{4.025+\delta}$ the conduction mechanism mainly follows band type conduction and small polaron hopping can be ignored [19–22]. We have elucidated the relationship between defect structure and thermodynamic quantities of LNAO [22]. The calculation of activity coefficient of holes showed that, like LNO, LNAO had a positive deviation from the ideal solution model and it was observed that oxygen nonstoichiometry of LNAO can be explained with a regular solution approximation [22]. Continuing on our previous work, in this work we have analyzed the electrical conductivity of LNAO in relation with the thermoelectric power (Seebeck coefficient) to elucidate the positive deviation of the activity coefficient of holes. The electrical conductivity relaxation measurement was used to calculate diffusion coefficient and surface exchange coefficient in order to analyze the oxygen exchange kinetics of LNAO. The electrical conductivity, and thermoelectric power measurements were performed as functions of temperature and pO_2 in $25 \leqslant T/^oC \leqslant 1000$ and $-14 \leqslant \log(pO_2/\text{atm}) \leqslant -1$ range, respectively. Also, conductivity relaxation was analyzed in $600 \leqslant T/^oC \leqslant 1000$ range and $-1.73 \leqslant \log(pO_2/\text{atm}) \leqslant -2.27$ range. The dilatometry was performed to analyze the expansion of LNAO from room temperature to 1050 °C range.

2. Experimental

2.1. Powder synthesis and sample preparation

Al^{3+}-doped LNO powder was prepared using lanthanum(III) acetate hydrate (99.9%, Aldrich, USA), nickel(II) acetate tetrahydrate (98%, Aldrich, USA) and Aluminum acetate(Aldirich, USA) as the starting materials by a coprecipitation method similar to that previously reported [4]. Stoichiometric amounts of each component were dissolved in distilled water and mixed together. A small amount of ammonium hydroxide was added to the system to adjust the pH to 10. The solution was dried under stirring condition and calcined at 900 °C for 5 h in air. The precalcined powder was then planetary ball-milled with stabilized zirconia balls for 3 h at 350 rpm. The dry power was calcined at 1100 °C for 5 h in air. The as-calcined powder was planetary ball-milled with stabilized zirconia balls for 3 h at 350 rpm and then was used for further analyses. Sample used for various measurements

* Corresponding author. Tel.: +82 62 530 1706; fax: +82 62 530 1699.
E-mail address: song@chonnam.ac.kr (S.-J. Song).

0925-8388/$ - see front matter © 2013 Elsevier B.V. All rights reserved.
http://dx.doi.org/10.1016/j.jallcom.2013.12.039

were prepared by molding the LNAO powder in the form of pellets/bars and then cold isostatically pressing at 150 MPa and sintering at 1350 °C in air. As-sintered samples were polished with 2000-grit SiC paper.

2.2. Physical characterization

The as-calcined powder was characterized by X-ray diffraction (XRD; D/MAX Ultima III, Rigaku, Japan) equipped with a Cu target X-ray tube at a scan rate of 1°/min between scanning angles of 10–90°. The obtained XRD pattern was refined using the Full-Prof program according to the Rietveld method. The microstructure of the fractured section of the sintered pellets was analyzed using a field-emission scanning electron microscope (FE-SEM, S-4700, Hitachi).

2.3. Dilatometry

A parallelepiped specimen ($3 \times 3 \times 11.9\ mm^3$) of $La_2Ni_{0.95}Al_{0.05}O_{4.025+\delta}$ was prepared 1350 °C sintered block. Thermal expansion was measured using a Netzsch L75 PT1600 dilatometer from room temperature to 1000 °C at 3 °C/min with an air gas at a flow rate of 200 cc/min.

2.4. Electrical conductivity and thermoelectric power measurement

The electrical conductivity and thermopower were measured by a standard, four-probe DC method using a measurement system including a digital multimeter (Keithley 2700) combined with a programmable current source (Keithley 6220). For the DC relaxation measurements, a specimen was completely equilibrated in a given thermodynamic condition and then the oxygen chemical potential was abruptly altered while recording the specimen's electrical conductivity vs. time until a new equilibrium was reached. The change in pO_2 was kept sufficiently small in order to regard the chemical diffusivity as constant.

For the thermoelectric power measurement, one side of the specimen was heated in a cell made of recrystallized alumina with a small Pt-wound sub-heater to generate a temperature gradient across the specimen. The thermal voltage, E, was measured by steady state technique at 5 levels of the temperature difference between 1 and 10 K with the aid of Pt-electrodes, Pt-lead wires and S-type thermocouples. The Seebeck coefficient for the specimen was determined from the slope of ΔE and the temperature difference after compensating for the thermopower of Pt as reported by Cusack and Kendall [23]. The overall measurements were repeated over the pO_2 range of $10^{-15} < pO_2/atm \leqslant 0.21$ in equilibrium state at various temperatures. The pO_2 was controlled by N_2/O_2 or 200 ppm CO balance by CO_2/CO_2 or CO/CO_2 mixtures and monitored by an ex situ zirconia-based oxygen sensor.

3. Results and discussion

Fig. 1 shows XRD pattern of 1100 °C as-calcined LNAO powder. As can be seen, all diffraction peaks can be assigned to a single-phase, orthorhombic layered perovskite structure (space group, 69 Fmmm) of LNO. No extra peaks of any other planes were detected, indicating the high purity of the product. The obtained XRD pattern was refined using the Full-Prof program according to the Rietveld method, and is also depicted in Fig. 1. The unit cell parameter obtained from the refined XRD pattern was $a = 5.438$, $b = 5.44$ and $c = 12.634$ Å, which indicates that there is an overall shrinkage in the unit cell of LNO on doping with Al^{3+}, as the lattice parameters of LNO were ($a = 5.453$, $b = 5.46$ and $c = 12.682$ Å) [19].

Fig. 2 shows SEM image of fractured cross-section of the LNAO pellet sintered at 1350 °C. As can be seen, the sintered specimen is fairly dense (~95% of theoretical density) with well-developed grains having grain size of 2–3 μm.

It is reported [24,25] that the LNO based systems observe only thermal expansion/contraction and they do not observe any significant chemical expansion/contraction on changing the thermodynamic conditions. Due to the layered nature of the structure of LNO system, oxygen loss from the LNO structure results in expansion along the perovskite-like layer due to the decrease in Ni oxidation state, but, at the same time, there is a contraction along the perpendicular c-axis due to the decrease in the concentration of oxygen ion interstitials. Therefore, no significant strains are developed over the range of oxygen hyperstoichiometry. Nevertheless, Fig. 3 shows the thermal expansion of LNAO, in terms of relative elongation, as a function of temperature. It is clear that LNAO exhibits a linear expansion without any discernible inflexion over the temperature range of 30–1000 °C. Data for LNO [20] are also plotted in Fig. 3 for comparison and, as can be seen, the thermal expansion curve for LNO almost overlaps to that for LNAO. In the temperature range under study, the average thermal expansion coefficient for LNAO and LNO are $13.77 \times 10^{-6}\ K^{-1}$ and $13.65 \times 10^{-6}\ K^{-1}$, respectively.

Fig. 4 shows the variation of the equilibrium total conductivity of LNAO as a function of temperature (Fig. 4a) and pO_2 (Fig. 4b). As can be seen, up to ~700 °C, LNAO shows a semiconductor-type behavior and total conductivity increased with increasing temperature. The activation energy for electrical conductivity is 0.09 eV, which is comparable to the other mixed ionic-electronic conductor, such as $La_{1-x}Sr_xCo_{1-y}Fe_yO_3$ [26]. At the higher temperatures 700 °C, however, a metallic behavior is observed and the total conductivity decreased with increasing temperature, which is attributed to the reduction of hole concentration leading to the loss of the interstitial oxygen [22]. Data for LNO [20] are also plotted in Fig. 4(a) and, as can be seen, the equilibrium conductivity for LNO follows similar trend and the activation energy was 0.07 eV at temperatures 700 °C. The variation of equilibrium total conductivities at different temperatures as a function of pO_2 in Fig. 4(b) shows that the conductivity increases with increasing activity but with ever-decreasing power to the oxygen activity, which is in agreement with previous reports [14,15,18]. At isothermal condition, the

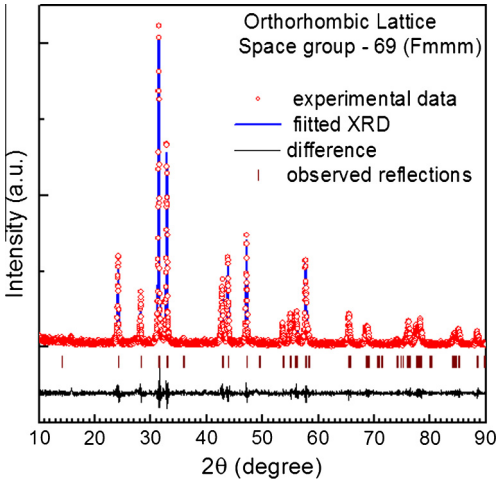

Fig. 1. XRD pattern of LNAO powder calcined at 1100 °C in air.

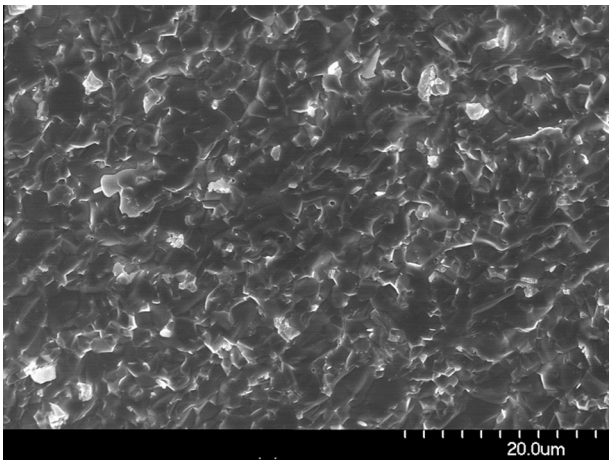

Fig. 2. SEM image of fractured cross-section of the LNAO pellet sintered at 1350 °C in air.